Imprinted Polymer Microrings as High-Performance Ultrasound Detectors in Photoacoustic Imaging

Cheng Zhang, *Student Member, IEEE, Member, OSA*, Sung-Liang Chen, Tao Ling, and L. Jay Guo, *Senior Member, IEEE*

(Invited Paper)

***Abstract*—Development of both fundamental research and clinical applications of photoacoustic imaging call for ultrasound detectors of high sensitivity, flat frequency response, and compact size, which are not easily satisfied by traditional ultrasound detectors. Therefore, many alternative ultrasound detectors have been investigated in recent years and a representative one is the imprinted polymer microring resonator-based detector. This review covers its principle, device fabrication, characterization and application, with an emphasis on how the microring's unique properties make it act as a high-performance ultrasound detector in photoacoustic imaging systems. The imprinted polymer microring has high detection sensitivity, broadband frequency response, compact size, and good operation robustness. Application of microrings in photoacoustic tomography generates truthful reconstructed images; use of microring in photoacoustic microscopy leads to improved image resolution; and the detector's compact size makes it promising for photoacoustic endoscopic applications. When integrated with other electromagnetic wave absorbers, novel applications such as real-time terahertz pulse detection can be realized.**

***Index Terms*—Microring resonators, nano-imprint, optical ultrasound detectors, polymer-based photonic devices, photoacoustic imaging, photoacoustic tomography, photoacoustic microscopy, photoacoustic endoscopy, real-time THz detection.**

I. Introduction

PHOTOACOUSTIC imaging (PAI), an elegant combination of light and sound, has been a research topic of great interest since the last decade [1]. In PAI, the object absorbs the incident electromagnetic (EM) waves (in most cases, laser light), and gets heated up. The heating causes the thermoelastic expansion of the object and subsequent generation of ultrasound waves (this process is called the photoacoustic effect). Finally, the ultrasound signals are collected for the subsequent image formation. Photoacoustic effect, in the general sense, can be described as the production of acoustic signals by any forms of EM radiation, ranging from X-rays to radio frequency waves. Although it was discovered over a century ago by A. G. Bell in 1880 during his experiments with the long distance sound transmission system (photophone) [2], PAI started to emerge as a new biomedical imaging modality in the last decade thanks to the development of various pulsed laser sources [3]–[5] and imaging reconstruction algorithms [6]–[9].

Compared with the traditional ultrasound imaging which relies on the acoustic impedance mismatch between tissues for the image formation [10], [11], PAI utilizes the optical absorption of either exogenous contrast agents such as dyes, nanoparticles, or the endogenous absorption contrast of biological tissues such as hemoglobin, lipid, melanoma, etc. As a result, PAI offers broad and great contrast in the detection of light-absorbing chromophores compared with the conventional ultrasound imaging [12]–[14]. By choosing proper excitation laser wavelengths, various tissues with different absorption spectra could be selectively mapped [15], [16]. Since tissue absorption is sensitive to its physiological status such as blood volume, oxygen consumption, etc, PAI is capable of interpreting metabolic and hemodynamic changes [17], [18]. Besides, compared with the pure optical imaging, PAI offers greater penetration into the biological tissues due to the significantly reduced scattering and attenuation of the acoustic wave than its optical counterpart [1], [17]. What is more, PAI can be combined with ultrasound imaging [19]–[23] or fluorescence imaging [23]–[26] to achieve complementary details to each other.

Ultrasound detectors play a vital role in PAI. For example, in photoacoustic microscopy (PAM), its axial resolution is inversely proportional to the detector bandwidth and can be estimated by: $\mathrm{R} = 0.88\,\mathrm{c}/\mathrm{BW}$, where R is the axial resolution, c the sound speed, and BW the detector's bandwidth [27]. Since c is a constant in most soft biological tissues, R is primarily determined by the detector's bandwidth. As an another example, for truthful image reconstructions in the photoacoustic tomography, both high frequency signals generated from the sharp parts of the object and low frequency signals from the smooth parts of the object need to be collected efficiently [28]. This requires an ultrasound detector with broadband response covering both low and high frequencies. Piezoelectric transducers have been the most commonly used ultrasound detector in PAI [29], [30]. They are usually operated over a band of frequencies centered at their resonant frequencies where the thickness of the piezoelectric crystal equals to half of the detected acoustic wavelength. As a result, high-frequency transducers require thin crystals, which impose demanding fabrication challenges and robustness issues. Thus, the axial resolution in the PAM stays around 15–20 μm [26], [31], and is one order of magnitude worse than

Manuscript received May 21, 2015; revised July 14, 2015 and August 7, 2015; accepted August 8, 2015. Date of publication August 10, 2015; date of current version September 12, 2015. C. Zhang, S.-L. Chen, and T. Ling contributed equally to this work. This work was supported by National Institutes of Health and National Science Foundation under Grant DBI-1256001.

The authors are with the Department of Electrical Engineering and Computer Science, University of Michigan, Ann Arbor MI 48109 USA (e-mail: chengzh@umich.edu; sungliang.chen@sjtu.edu.cn; taoling@umich.edu; guo@umich.edu).

Color versions of one or more of the figures in this paper are available online at http://ieeexplore.ieee.org.

Digital Object Identifier 10.1109/JLT.2015.2466661

0733-8724 © 2015 IEEE. Personal use is permitted, but republication/redistribution requires IEEE permission.
See http://www.ieee.org/publications_standards/publications/rights/index.html for more information.

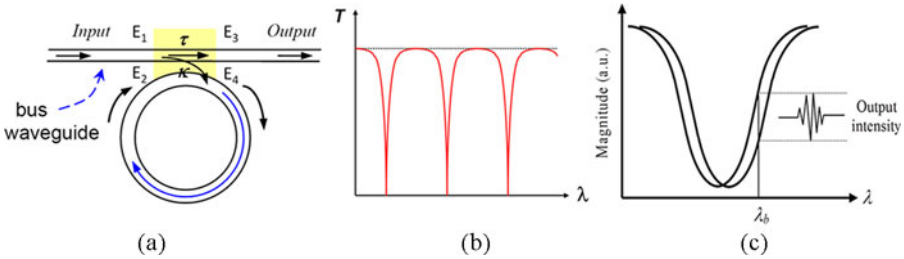

Fig. 1. (a) Schematic drawing of the microring resonator, consisting of a ring waveguide coupled to a straight bus waveguide; (b) Transmission spectrum of the microring; (c) Ultrasound detection by the microring sensor. Reproduced with permission from [39]. Copyright 2008 IEEE.

the lateral resolution achieved by fine laser focusing [32], [33]. Moreover, a broad acoustic bandwidth covering nearly DC to very high frequencies, which is essential to truthful image reconstructions, is highly restricted due to the characteristic of this resonance effect. What is more, in order to move PAI towards clinical applications, detectors need to be compact in size, robust to operate and immune to the EM interferences [34]–[36]. Unfortunately, many of the above characteristics are not easily satisfied by the conventional piezoelectric transducers. To solve the above limitations, alternative ultrasound detectors have been developed, such as optical resonator based ultrasound detector [37]–[40], capacitive micro-machined ultrasonic transducers (CMUTs) [41], [42].

In this review, an optical resonator based ultrasound detector—the imprinted polymer microring is discussed. The detector's working principle, design and fabrication are discussed at first, followed by its characterization. The polymer microring ultrasound detector has high sensitivity, broad bandwidth, wide angular tolerance, robustness of operation and the potential for array integrations. Its advantages are further illustrated by the various applications in PAI. The high sensitivity and broad bandwidth benefit the image resolutions in the PAM; the wide angular tolerance and broad bandwidth enhance truthful image reconstructions in the photoacoustic tomography; the device's tiny foot print makes it promising for clinical endoscopic applications. When integrated with EM wave absorbers such as carbon nanotubes, novel applications such as real time THz wave detection via the photoacoustic effect is achieved.

II. Principle

A microring resonator consists of a ring shape waveguide coupled with a straight waveguide and there is light coupling in and out of the ring in the gap region (see Fig. 1(a)) [43]. Microring of such a configuration can be treated as a miniature Gires–Tournois etalon (reflection type Fabry–Perot interferometer). By sweeping the input laser wavelength, the microring's output intensity dip occurs at specific wavelengths when the corresponding round trip phase accumulation in the ring waveguide equals to multiples of 2π radians (see Fig. 1(b)). This round trip phase accumulation depends on many parameters such as the ring radius, cross-section size, refractive index of the polymer waveguide core/cladding, etc, all of which can affect the effective index of the propagating mode. When the ultrasound waves are incident onto the polymer microrings, the polymer refractive index can be modulated through the elastic-optic effect (Strain creates a proportional perturbation of the refractive index in the medium [44]). At the same time, the ring is deformed by the ultrasound waves, affecting the effective index of the propagating waveguide mode. These two effects altogether influence the ring resonant wavelength. By setting the probe laser wavelength at the slope of the ring transmission dip, the incident ultrasound waves could be recorded by the varying output intensity from the device (see Fig. 1(c)).

The sensitivity of the polymer microring to an acoustic pressure can be expressed as [45]:

$$S = \frac{dT}{dP} = \frac{dT}{d\lambda}\frac{d\lambda}{dn_{\text{eff}}}\frac{dn_{\text{eff}}}{dP} \tag{1}$$

where T and P are the optical transmission intensity and acoustic pressure amplitude, respectively. The first derivative $\frac{dT}{d\lambda}$ represents the change in the device transmission intensity for a certain resonant wavelength shift at a fixed probing laser wavelength. This quantity is closely related to the sharpness of the resonance curve, denoted by the quality factor (Q factor) of the microring. The second derivative $\frac{d\lambda}{dn_{\text{eff}}}$ is the resonance wavelength shift with respect to the change of the effective refractive index and is a constant when the resonant wavelength shift is tiny. The third term $\frac{dn_{\text{eff}}}{dP}$ is a parameter signifying how sensitive the polymer properties change with respect to the ultrasonic pressure and can be described in terms of the Young's modulus and the elastic-optic coefficient. Therefore, the microring detector's sensitivity depends on its Q factor as well as the polymer properties.

III. Fabrication

The polymer microring is fabricated by the nano-imprint lithography [46]. In nano-imprint, a mold is pressed into the polymeric materials cast on a substrate in a controlled fashion (such as certain temperature, pressure and with ultraviolet light irradiation, etc). After their separation, an inverse replica of the mold pattern will be created on the polymer material. Compared with alternative methods such as the electron beam/photo lithography (or with combination of etching) to fabricate polymer based photonic devices, nano-imprint has the advantages of simplified process, increased throughput, and improved reproducibility. More importantly, by taking additional steps during the mold preparation (as discussed in the next paragraph), molds with smooth side wall profiles can be fabricated and this contributes to the high quality factor (Q factor, defined as $Q = \lambda/\Delta\lambda$, where λ is the device working wavelength and $\Delta\lambda$

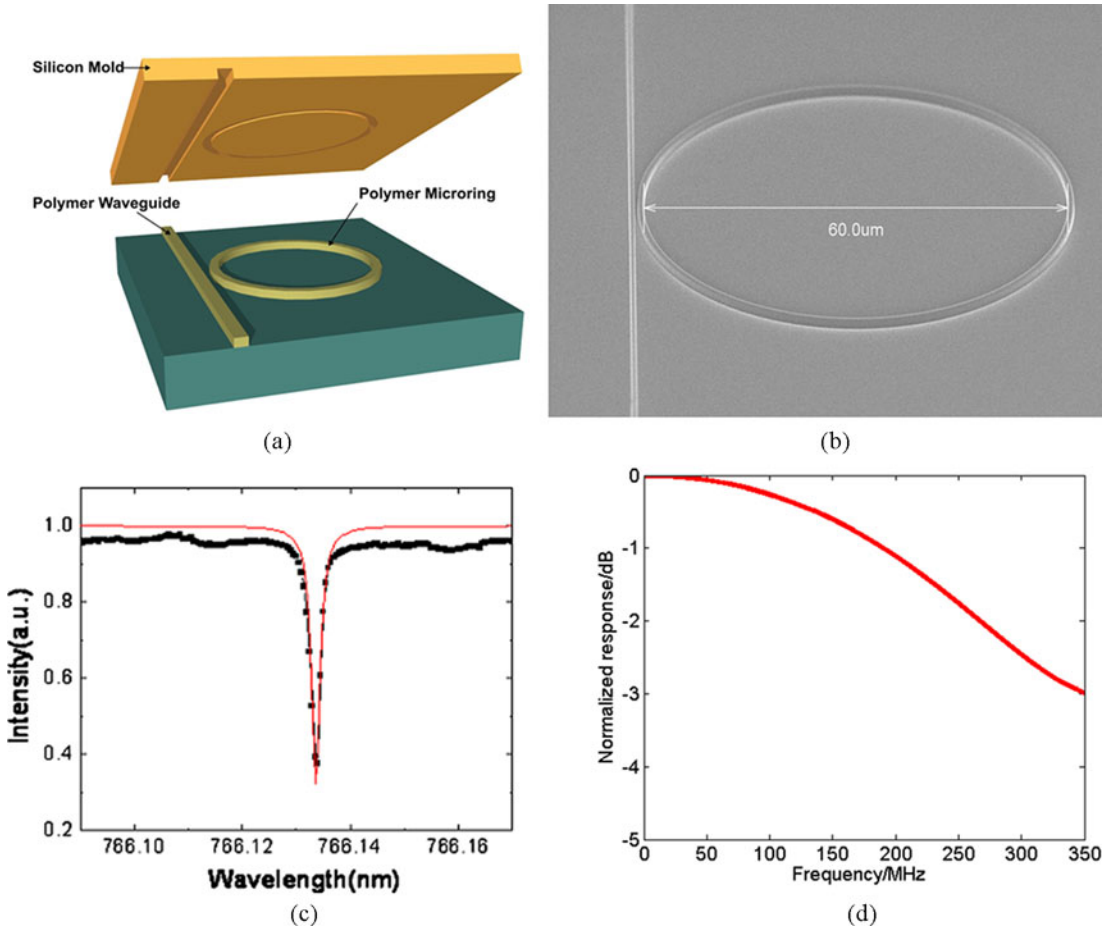

Fig. 2. (a) Polymer ring fabrication schematic by nano-imprinting lithography. (b) Angle view SEM of the microring with a diameter of 60um; Reproduced with permission from [52]. Copyright 2014 American Chemical Society. (c) Transmission spectrum of microring around 780 nm with a Q factor of 4×10^5 in DI water; Reproduced with permission from [37]. Copyright 2011 AIP Publishing LLC. (d) Measure frequency response of the microring, and it has broad response from DC to 350 MHz at -3 dB. Reproduced with permission from [52]. Copyright 2014 American Chemical Society.

is the FWHM of the transmission dip) of the imprinted polymer microring. High Q factor is valuable for microring's application as ultrasound detectors because for a given acoustic pressure, the amplitude of the resonant wavelength shift is proportional to the Q factor. A higher Q factor means sharper resonance, thus being more sensitive to the acoustic vibration.

The device fabrication starts with the imprint mold preparation. Silicon is chosen as the mold material for its wide availability and varieties of relevant fabrication processes. In particular, recent developments in silicon dry etching produce smooth sidewall profiles [47]–[49]. First of all, electron beam (E-beam) lithography (Raith 150) is used to define the device pattern on polymethyl methacrylate (950K, PMMA) spun on a Si substrate. Rather than directly using PMMA as an etching mask to transfer the pattern into the Si substrate after E-beam, PMMA goes through a reflow treatment (115 °C for 90 s), which can significantly reduce the imperfections in the PMMA resist and harden its edges [50], [51]. Thus, there are fewer defects when transferring the pattern from PMMA into the Si substrate through the plasma coupled reactive ion etching (RIE). After thermal reflow, the PMMA is used as the mask in the C_4F_8 and SF_6 gas based RIE to transfer the pattern into the Si substrate. After etching, the PMMA is removed by acetone. To further reduce the sidewall roughness of the mold and improve the imprinted device performance, there is a second important step: silicon thermal oxidation followed by the buffered hydrofluoric acid (BHF) etching, where the outside layer of the rough Si on the mold is converted to SiO_2 during the thermal oxidation and subsequently removed by the BHF. After this treatment, the Si mold sidewall roughness is significantly reduced [50]. The mold is finally employed in a thermal imprinting process on polystyrene (PS) film spun on a thermal oxide substrate (acts as the bottom cladding), as shown in Fig. 2(a). The imprinting is done at 180 °C under 600 PSI pressure for 5 minutes (Nanonex NX-2000). Fig. 2(b) shows a scanning electron microscope (SEM) picture of the imprinted microring, and Fig. 2(c) is the measured transmission spectrum around 780 nm in di-ionized (DI) water with a Q factor of 4×10^5. For some applications such as photoacoustic computed tomography [1], [17], photoacoustic signals are detected at different locations (e.g., a circular configuration) and used for the subsequent image reconstruction. Parallel detection using a microring array gives faster signal capture speed than scanning a single ring element over different positions. We did preliminary demonstrations of a four-element microring array by fabricating microrings of slightly different diameters

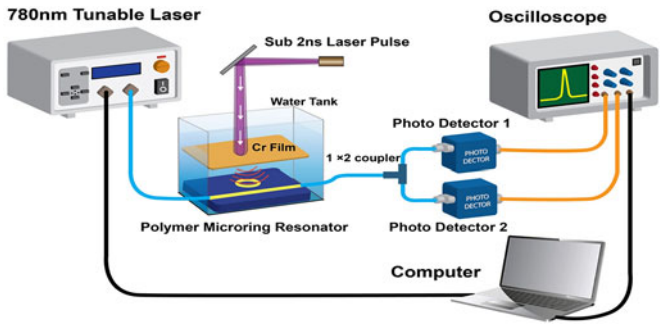

Fig. 3. Typical experiment set-up to operate the polymer microring in PAI. In biological experiments, the Cr film will be replaced by tissues. Reproduced with permission from [52]. Copyright 2014 American Chemical Society.

coupled with the same bus waveguide [39]. By varying the input laser wavelength, individual ring will be addressed (similar to the concept of wavelength multiplexing). In order to make denser array, smaller size rings are needed. Reduction in ring size leads to increased bending loss and reduced Q factor (ring material-polystyrene is transparent at its working wavelength, and therefore there is no material loss in this case). To solve the above issue, we have investigated imprinted polymer microrings on metallic or high refractive index substrates, which show significantly improved Q factors compared with those of microrings on thermal oxide substrates [45].

IV. Characterization

After the device is fabricated on a chip, its input and output ends are cleaved and then glued to optical fibers. Fig. 3 shows the schematic drawing of a typical set-up for microring operations. In this set-up, the photoacoustic signal is generated by shining a ns laser (GL-3300, Photon Technology International) onto a 200 nm thick Chromium (Cr) film (In PAI experiment, the Cr film is replaced by the biological tissues). A continuous-wave (CW) 780 nm tunable laser (TLB-6312, New Focus) is coupled into the device input fiber and its output fiber is connected to a 1×2 coupler with 90:10 split ratio (FCMM50–90A-FC, Thorlabs). The outputs of the coupler are detected by two photo-detectors and finally recorded by a digital oscilloscope (DSO7054A, Agilent). To lock the probing wavelength at the sharp slope of the ring resonance spectrum, output from the 10% channel of the coupler is monitored by one photodetector (1601, New Focus) and used for feedback control of the tunable laser. While the rest 90% of output is collected by a high-speed avalanche photo detector (APD210, Menlo Systems) and used for photoacoustic signal detections. The device is immersed in DI water which served as both the top cladding of the microring and the coupling medium for the ultrasonic propagation.

The detector acoustic sensitivity is calibrated against known acoustic sources such as ultrasound transducers [50]. One parameter for evaluating the detector performance is the noise-equivalent pressure (NEP), i.e., the minimum detectable pressure right above the system noise level. We recently achieved a NEP of 105 Pa from 1–350 MHz range [52]. Another distinctive advantage of the polymer microring is its ultra-broad detection bandwidth. The ring frequency response is calibrated by measuring its response to a broadband ultrasound signal, generated by a 200 nm Cr film irradiated by a nanosecond laser pulse [8], [52], as shown in fig. 3. Fig. 2(d) shows the calibrated response bandwidth of ring. It has a flat response stretching from DC to $\sim$350 MHz at -3 dB (0.707). A Gaussian function is used to extrapolate the ring response spectrum and gives out -6 dB response at 470 MHz. This corresponds to a FWHM bandwidth of 940 MHz and an estimated axial resolution of 1.4 μm (R $= 0.88$ C/BW). Lastly, the tiny size of microring makes it behave like a point detector with wide angular response, a property useful for photoacoustic tomography and beam forming applications [28], [53]. The sensor's angular detection sensitivity can be theoretically described by considering a ring shape transducer: $\mathrm{D}_0 = \mathrm{J}_0(\mathrm{ka}\sin\theta)$, where J_0 is the zero order Bessel function of the first kind, k is the wave-vector of the incident acoustic wave, a is the radius of the microring and θ the incident angle of the acoustic wave. For a given D_0 and acoustic wave-vector k, smaller radius a leads to a larger θ (wider angular response). We demonstrate $-$6dB response over 40º for 30 MHz acoustic waves using a microring with 40 μm diameter [37].

Besides the high sensitivity, ultra-broad detection bandwidth and wide angular response, microring resonators have relatively size-independent detection sensitivity, and are robust against the EM interference as well as ambient noise. And they can be potentially integrated into arrays [39], [45], leading to a faster imaging speed. All these advantages facilitate PAI and sensing applications, which would be discussed in the following part.

V. Optical Resonator Based Ultrasound Detectors

As mentioned earlier in the introduction part, there is an increasing demand for alternative ultrasound detectors by their unique advantages over traditional piezoelectric transducers. Examples include capacitive micro-machined ultrasound transducers (CMUTs), optical resonator based ultrasound detectors (ORUDs), etc. Compared with the piezoelectric transducer, CMUT is the detector where the ultrasound energy transduction is due to the change in its capacitance [54], [55]. It is compatible with the current silicon micro-fabrication technology and suitable for array integrations [42], [56], [57]. ORUD are based on optical resonances, and their resonance behaviors can be modulated by the ultrasound waves. Thanks to the various forms of optical resonant phenomena and structures, researchers can build different ultrasound detectors according to their needs. Besides the polymer microrings, Si based microrings [58] and waveguides [59], [60] are also demonstrated for ultrasound detections. The Si microring consists of a suspended ring cavity which works simultaneously as an acoustic resonating structure. It offers ultrahigh detection sensitivity (below 1 Pa at 0.75 MHz) with limited bandwidth. Monifi *et al.*, showed acoustic wave detection using a fiber coupled silica microtoroid resonator encapsulated in a polymer surrounding [61]. Fabry–Perot cavity has been a popular platform for researchers to build ORUDs [62]–[66]. It consists of a polymer layer sandwiched by two reflective mirrors. The probe laser beam undergoes multiple reflections within the cavity and the optical resonance establishes when its round trip phase accumulation equals to multiples of 2π radians. The incident ultrasound waves modulates the thickness of the polymer film and thus changes the cavity

resonant wavelengths. Fabry–Perot cavity based ultrasound detectors can be operated in either reflection [66] or transmission [67] mode, and can be integrated on the tip of a fiber, which is well suitable for endoscopic PAI applications [38], [68], [69]. Comparatively speaking, the microring resonators offers higher resonant Q factor than the Fabry–Perot resonator, especially if the propagation loss inside the ring waveguide is reduced. While the Fabry–Perot cavity requires special mirror designs in order to achieve high Q.

So far, several ORUDs besides the polymer microring have been employed in PAI systems. Ashkenazi *et al.*, used a thin (10 μm) SU8 polymer Fabry–Perot étalon to demonstrate high resolution imaging of a microsphere phantom [62]. Huang *et al.*, and Hou *et al.*, extended to 3D imaging by using a two dimensional (2D) SU8 Fabry–Perot sensor arrays [63], [64]. Zhang *et al.*, reported a planar Fabry–Perot polymer film ultrasound sensor for high-resolution 3D imaging of a blood vessel phantom [70]. Paltauf *et al.*, proposed a Mach–Zehnder interferometer as an acoustic line detector for 3D photoacoustic tomography [71]. Nuster *et al.*, constructed such interferometers through free space propagating laser beam for PA wave monitoring [72]. Hochreiner *et al.*, demonstrated remote PAI of biological samples using a two wave mixing interferometer [73]. Wang *et al.*, reported a noncontact PAM technique by detecting PA signals using a low coherence interferometer, a commonly used hardware in optical coherence tomography system [74]. Blatter *et al.*, demonstrated another noncontact PAM imaging via phase sensitive optical coherence tomography [75]. Gutierrez–Juarez *et al.*, detected melanoma cells using an optical reflectance method for PA waves detection [76].

VI. Applications

A. Photoacoustic Tomography

PAI is usually categorized into several different types: photoacoustic tomography (PAT), photoacoustic microscopy (PAM), and their variants. This classification is essentially based on the variations of methodologies in the data acquisition and image construction, rather than any fundamental differences in their mechanisms. PAT was developed earlier and is currently the most general PAI approach [7], [77]. In PAT, pulsed laser beam illuminates the tissue, covering the whole region of interest. Laser absorption by specific chromophores in the tissue converts the light energy to broadband ultrasonic waves through the photoacoustic effect. The generated acoustic waves are detected by either a mechanically scanned ultrasonic detector or an array of detectors. The time-domain ultrasonic waveforms carry spatial information of the absorbers inside the tissue and can be back-projected to reconstruct a three-dimensional (3D) image using the known sound speed. Three common scanning geometries are spherical, cylindrical, and planar configurations.

In additional to other optical resonator based platforms described in the last section, polymer microring resonators have been exploited for high-resolution PAT imaging [28], [53]. We demonstrated high quality PAT images using the circular scan by taking advantages of two outstanding characteristics of the microring sensors: broad bandwidth and wide angular response. First of all, wideband PA detection is essential for truthful image reconstructions of multi-scale objects, e.g., tissues of various sizes. As shown in Fig. 4, a simulation of 2D PAT of microspheres shows that objects with their boundaries of high spatial frequencies and the inner structure primarily of low spatial frequency components can be faithfully reconstructed using microring sensors with wide band response. In contrast, the images obtained by the piezoelectric transducers with limited bandwidth miss either the sharp boundary or the uniform inner region. Secondly, the wide acceptance angle of PA detection leads to less distortion at larger incident angles of acoustic waves, resulting in high resolutions over a large field of view. Thus, these properties make microrings excellent candidates for sensitive and wide-angle PA imaging applications. It is worth mentioning that unlike the piezoelectric transducers, the sensitivity of microrings primarily depends on its Q factor rather than the sensor size. We compared the imaging quality using different sizes of detectors with similar sensitivity and frequency response. The results, as shown in Fig. 5, show significantly improved imaging contrast and resolution over the whole imaging region using smaller size detectors.

B. Photoacoustic Microscopy

PAM refers to the PAI acquisition methodology by scanning either a focused ultrasound detector or a focused laser beam. Unlike PAT with the need of reconstruction algorithms, PAM image is directly presented by incorporating a series of received peak amplitude lines (commonly referred as A-lines). PAM can be classified into acoustic resolution PAM and optical resolution PAM. The former uses diffused laser radiation and focused ultrasound detectors. Its lateral resolution is determined by the characteristics of ultrasound propagation media and the detector [78]. In contrast, optical resolution PAM uses a focused laser beam and the lateral spatial resolution is decided by the spatial size of the focused laser beam, resulting in high lateral resolution if light is not severely scattered in deep tissues [33]. In both acoustic and optical resolution PAM, the axial resolution is related to the ultrasound detector bandwidth, and can be roughly estimated as: $R = 0.88$ C/BW (C is the sound speed and BW is the detector FWHM bandwidth) [27]. Optical resolution PAM provides excellent resolutions at a shallow depth of approximately 1 mm, and is well complemented by the acoustic resolution PAM which offers moderate resolutions at several centimeters depth.

Although optical resolution PAM achieves high lateral resolution (on the order of light wavelength) by a tightly focused laser spot, the axial resolution is on the scale of tens of micrometers due to the limited bandwidth of the piezoelectric detectors used in most PAM systems. Such resolutions define an asymmetric image voxel. With the merit of wideband frequency response, microrings could play an important role to make up for the laggard axial resolution. Besides, the high sensitivity of microrings is indispensable in PAM because the PA signals from small

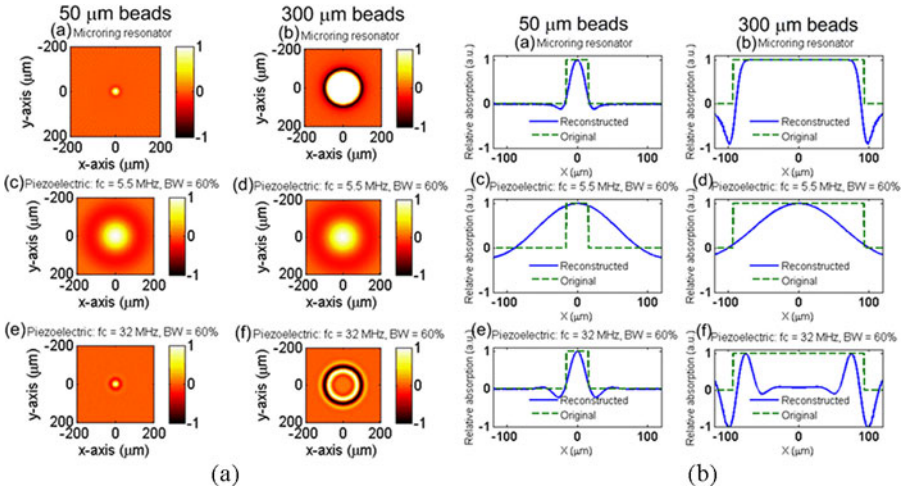

Fig. 4. (a) The reconstructed image of a 50 μm polystyrene (PS) bead (left column) and a 300 μm PS bead (right column) using microring resonator detectors, piezoelectric transducers with a central frequency of 5.5 MHz and 60% bandwidth, and piezoelectric transducers with a central frequency of 32 MHz and 60% bandwidth, respectively. Note that the effective sizes of the beads in water are 31.1 and 186.6 μm, respectively, considering the different sound speeds in PS (2380 m/s) and water (1480 m/s). (b) The line profile of the reconstructed image at $y = 0$ μm. The line profiles in (b) correspond to the 2D images in (a), respectively. Reproduced with permission from [28]. Copyright 2009 IEEE.

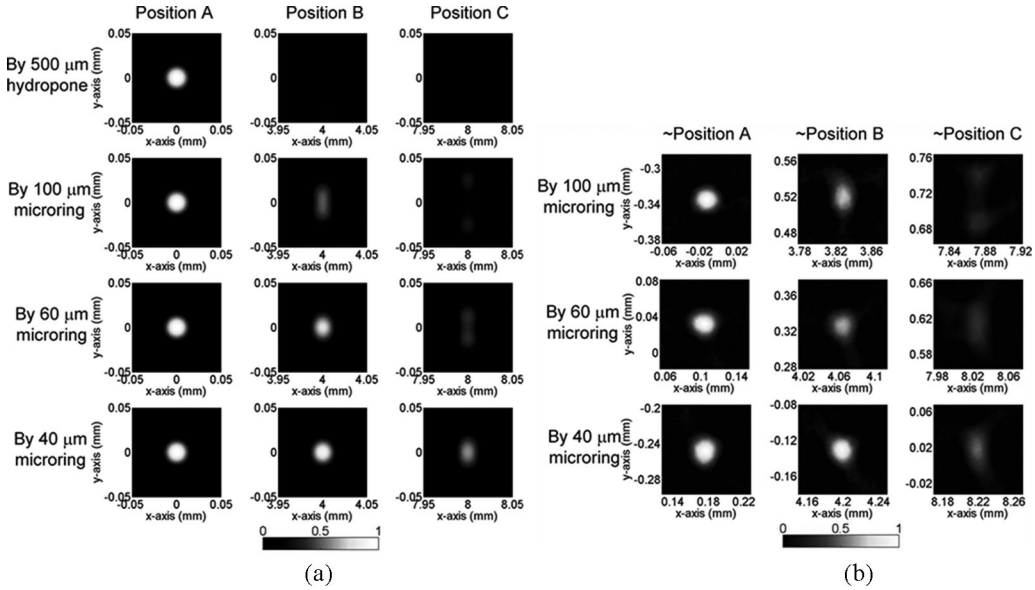

Fig. 5. (a) Simulated PAT images of 50 μm PS beads (effective size = 31 μm, as mentioned in Fig. 1) using different types and sizes of detectors with similar sensitivity. The scanning radius was 12 mm with a step size of 3 degree, and the scanning center was set as coordinates (0, 0) with three beads at coordinates A (0,0), B (4,0), and C (8,0) mm. (b) Experimental PAT images of 50 μm PS beads (effective size = 31 μm) using different sizes of microrings. Reproduced with permission from [53]. Copyright 2011 Society of Photo Optical Instrumentation Engineers.

objects, such as capillaries or individual red blood cells, are much weaker than those of PAT dealing mostly with the macroscale tissues such as large vasculatures. We constructed an optical resolution PAM by raster scanning a focused laser beam onto the imaging targets with microrings as PA sensors [79]. A 2 ns, 532 nm Nd: YAG pulsed laser (1 kHz repetition rate) is scanned over the sample (mouse bladder wall) in the XY plane. The laser light is focused into a spot of 5 μm (lateral resolution). Microring and traditional ultrasound transducers are used to collect the photoacoustic signals. The results for imaging vasculature in a mouse bladder wall *ex vivo* using microring and conventional transducer are shown in Fig. 6. Their image qualities are similar in the lateral direction, since the resolution is determined by the focused laser spot. However, there are significant differences in the images along the axial directions (XZ and YZ planes). Thanks to the broad bandwidth of the microring detector, the tissue axial profile is clearly resolved; in contrast, images acquired with a limited bandwidth transducer are blurred [79]. Therefore, the large bandwidth of the microring detector greatly benefits the image axial resolution. To demonstrate its capability of *in vivo* optical resolution PAM, the microring is used in imaging of the vasculatures in a mouse ear *in vivo*. Before imaging, 0.03 ml Ketaset with ketamine 100 mg/ml was injected to anesthetize the mouse and hairs on the ear were removed using hair-removing lotion (see Fig. 7(a)). The photoacoustic image of the vessels in the XY plane is shown in Fig. 7(b).

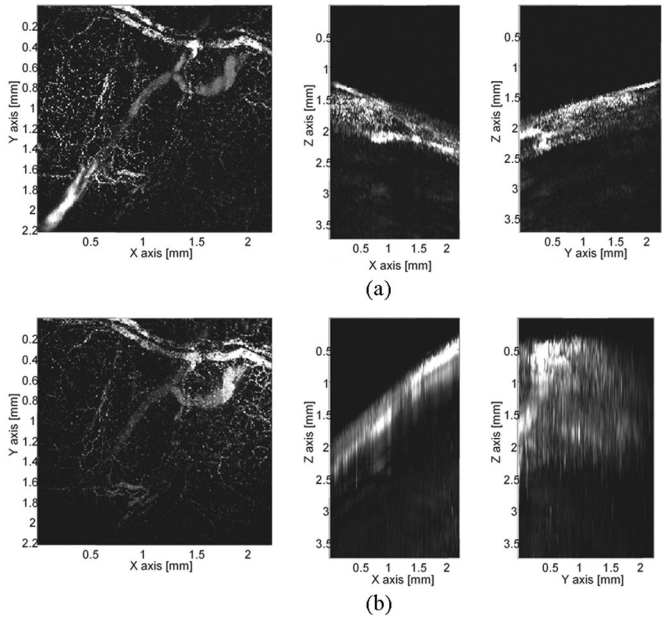

Fig. 6. Cross section images on XY, XZ, YZ planes of the vasculature in a mouse bladder wall *ex vivo* acquired using microring (row a) and conventional transducer (row b). Reproduced with permission from [79]. Copyright 2011 The Optical Society of America.

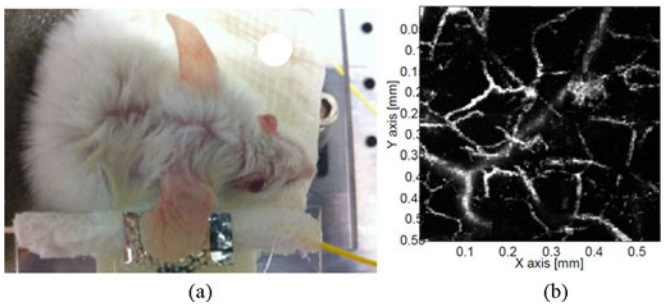

Fig. 7. (a) Photograph of a mouse ear sample. (b) Maximum amplitude projection (MAP) on the XY plane of the mouse ear *in vivo*. Reproduced with permission from [79]. Copyright 2011 The Optical Society of America.

C. Photoacoustic Endoscopy

With the rapid development of the PA imaging technology, several potential clinical applications have attracted increasing attention. In some of these applications, the target tissue can only be accessed by inserting a miniature endoscopic device through an inherent passage such as the esophagus, the urethra or the coronary artery. Numerous prototype PA endoscopic or intravascular devices have been developed by the piezoelectric detectors or ORUDs [36], [80]–[82]. Usually, ORUDs possess the advantages of small size, size-independent sensitivity, and immunity against EM interference, providing a unique fit to the demanding requirements of miniature probes for future *in vivo* applications. Moreover, these sensors can be probed through optical fibers with laser sources and photodetectors remotely connected, circumventing the challenges of integrating amplifier circuits for piezoelectric detectors in a limited space of the probe distal end.

The microring was incorporated to build an integrated intravascular ultrasound and PA imaging scan head [36], [83]. Additionally, it was exploited on an optical resolution PAM platform with a raster scan of the laser beam performed by a micro-electro-mechanical-systems (MEMS) mirror, which is used to meet the requirement of system miniaturization [84]. The system is capable of 3D imaging with high resolutions of 17.5 μm in lateral direction and 20 μm in axial direction. Anatomical photograph of the inner wall of a canine bladder is shown Fig. 8(a). The photoacoustic images on the XY and XZ planes of the microvasculature in the bladder wall obtained by the microring detector and the needle hydrophone are shown in Fig. 8(b) and (c), respectively. Microscopic imaging acquired by the microring detector has good spatial resolution, high contrast-to-noise ratio, and satisfactory continuity. We also fabricated a transparent microring resonator device for backward-mode PA endoscopy [85], which is important to future *in vivo* applications.

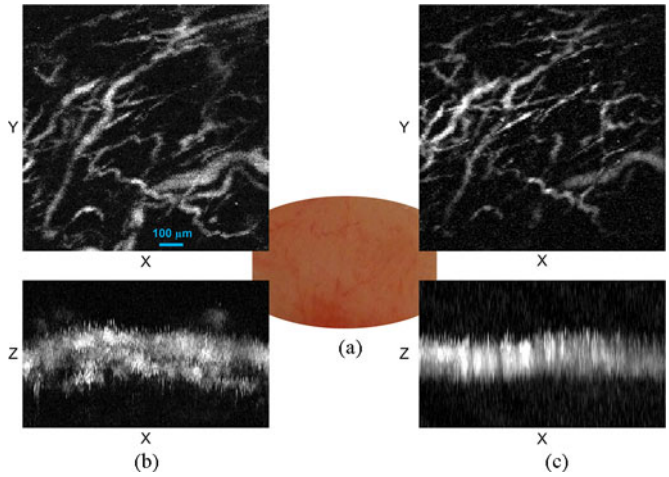

Fig. 8. (a) Anatomical photograph of the inner wall of a canine bladder. (b) MAP images on the XY and XZ planes of the microvasculature in the bladder wall obtained by microring detectors. (c) MAP images of the same area acquired by the needle hydrophone. All images share the same scale bar as shown in the left-upper image. Reproduced with permission from [84]. Copyright 2012 The Optical Society of America.

D. Photoacoustic Fluidics

Flow is an essential contrast, providing useful pathophysiological information. PA techniques in flowmetry and flow cytometry are receiving increased attention because the merits in PAI, such as deeper penetration depth in tissues than that by the pure optical counterpart [86]–[88]. Microring was utilized on a proposed flowmetry called PA correlation spectroscopy, in which auto-correlation is conducted to extract dynamic information [89]. The potential of this technique for measuring blood flow speed in capillaries was also illustrated.

E. Real Time Terahertz (THz) Pulse Detection

THz sensing plays an important role in industry, biology, and material science. Most existing techniques for THz detection either require bulky optics or need cryogenic cooling, and the un-cooled thermal detectors usually suffer from the long integration time. We have proposed and experimentally demonstrated a novel scheme based on photoacoustic detection of THz (PADTH) pulse radiation [90], [91]. According to the

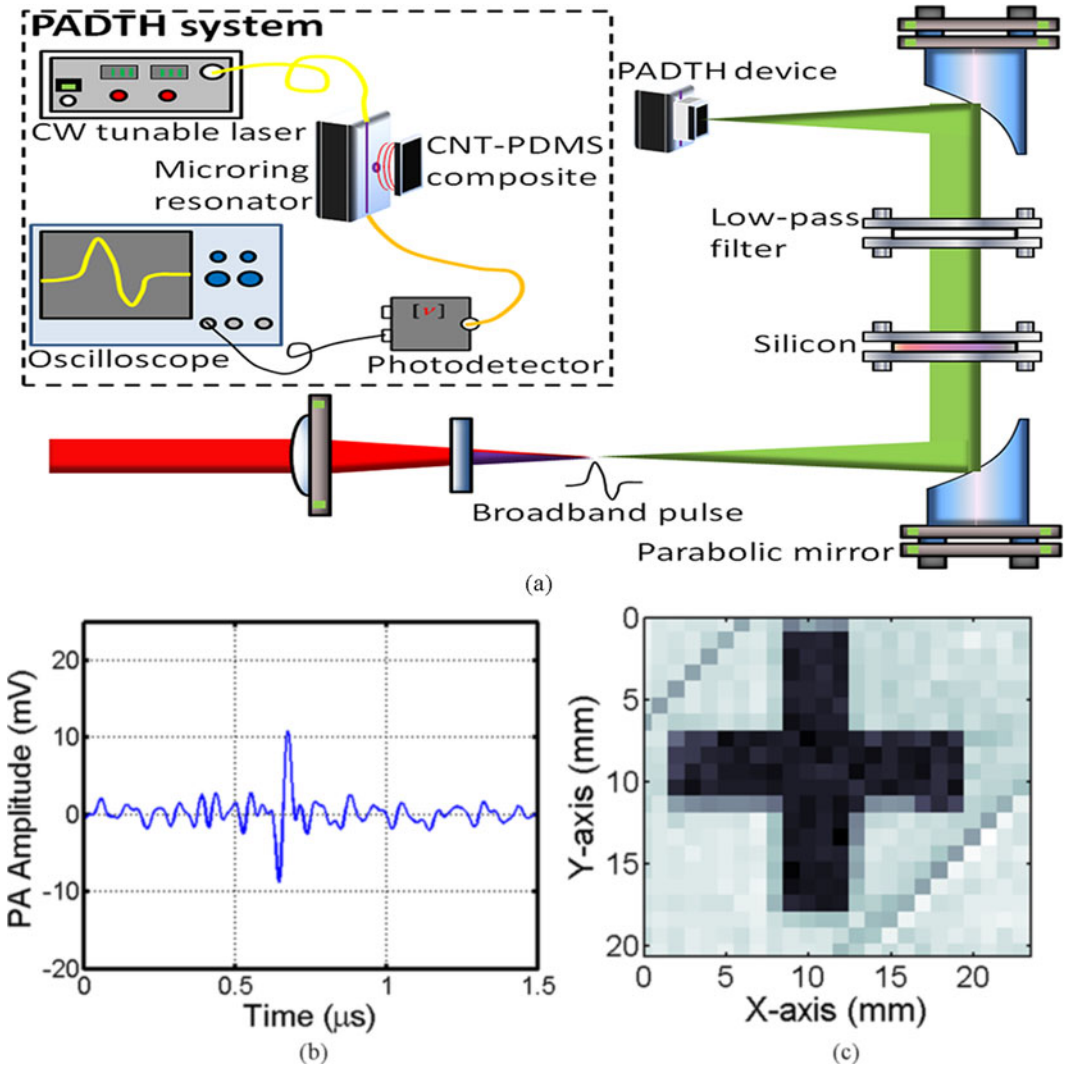

Fig. 9. (a) Experimental set-up of PADTH system; (b) Detected photoacoustic signal from signal THz pulse, signifying the system real-time response capability. (c) A THz image by PADTH system. Reproduced with permission from [90]. Copyright 2014 Nature Publishing Group.

previously mentioned description of the photoacoustic effect (the production of acoustic signals by any forms of EM radiation), the energy of individual THz pulses can be converted to acoustic waves with a proper light absorbing and thermal expansion medium (carbon nanotube-PDMS composite in our case [82]–[83]). In PADTH, the transient and localized heating in the carbon nanotube-PDMS composite by the absorption of THz pulse energy produces ultrasound, which is subsequently detected by a highly sensitive microring acoustic sensor (see Fig. 9(a)).

Different from the conventional thermal detectors utilizing continuous heat integration, this new method of THz detection responds to the energy of each individual THz pulse, enabling real time detection and imaging (see Fig. 9(b) and (c)). The detection speed of PADTH system is determined by the time to generate a photoacoustic signal and the detected acoustic signal duration. In this case, the detected acoustic pulse duration dominates, resulting in a response time of less than 0.1 μs. In contrast, bolometers reply on the electric resistance change with respect to the temperature variation and the response time is about 0.1 ms. What is more, bolometer operation usually requires cryogenic cooling that limits their wide applications. Pyroelectric detectors work at room temperature, but the response is even slower ($\sim$0.1 s) [90]. Electro-optical sampling can detect THz pulse at fast speeds, but the system is bulky [92]. Broadband THz absorption is possible by the extraordinary absorption of CNT-polymer composite across a wide spectrum range [93]–[95]. Besides, our method offers additional advantages of room-temperature operation, compact system size, robustness against ambient noise, etc.

F. Future Directions

Imprinted polymer microring has been applied in various PAI applications. To better facilitate its clinical applications, the ring size can be further reduced or the device can be integrated with a probe (especially for endoscopic applications) [68], [96]. Besides, to overcome the difficulties with the respiratory and cardiac motions of the live imaging subjects, the system should be capable of fast laser beam scanning and signal capture [31].

What is more, microring can be employed in multimodality imaging systems (e.g., photoacoustics, ultrasound, fluorescence, etc.) [22], [23].

VII. Conclusion

This review covers the design, fabrication and applications of the imprinted polymer microring as high performance ultrasound detectors in PAI and sensing systems. By carefully reducing the defects in the imprint mold, high Q (on the order of 10^5) polymer microring is fabricated. It has high ultrasound detection sensitivity, ultra-broad and flat frequency response from nearly dc to a few hundred megahertz, wide angular acceptance and robust operation. Applications of microring in PAI yield better results compared with traditional ultrasound detectors: improved axial resolution in photoacoustic microscopy, faithful image reconstruction in photoacoustic tomography. The compact size of the microring is also suitable for endoscopic and intravascular PAI systems. Based on the principle of the photoacoustic effect, real time THz pulse detection is achieved by absorbing the THz pulse with CNT-PDMS composite and the subsequent ultrasound signal detection with microrings. New device structures and applications are to be explored in the future.

References

[1] L. V. Wang and S. Hu, "Photoacoustic tomography: In vivo imaging from organelles to organs," *Science*, vol. 335, pp. 1458–1462, Mar. 2012.

[2] A. G. Bell, "On the production and reproduction of sound by light," *Amer. J. Sci.*, vol. 20, pp. 305–324, Oct. 1880.

[3] L. Zeng, G. Liu, D. Yang, and X. Ji, "3D-visual laser-diode-based photoacoustic imaging," *Opt. Exp.*, vol. 20, pp. 1237–1246, Jan. 2012.

[4] Y. Wang, K. Maslov, Y. Zhang, S. Hu, L. Yang, Y. Xia *et al.*, "Fiber-laser-based photoacoustic microscopy and melanoma cell detection," *J. Biomed. Opt.*, vol. 16, pp. 011014-1–011014-4, Jan./Feb. 2011.

[5] E. Holthoff, J. Bender, P. Pellegrino, and A. Fisher, "Quantum cascade laser-based photoacoustic spectroscopy for trace vapor detection and molecular discrimination," *Sensors*, vol. 10, pp. 1986–2002, Feb. 2010.

[6] X. Minghua and L. V. Wang, "Time-domain reconstruction for thermoacoustic tomography in a spherical geometry," *IEEE Trans. Biomed. Imag.*, vol. 21, no. 7, pp. 814–822, Jul. 2002.

[7] L. V. Wang, "Tutorial on photoacoustic microscopy and computed tomography," *IEEE J. Sel. Topics Quantum Electron.*, vol. 14, no. 1, pp. 171–179, Jan./Feb. 2008.

[8] G. J. Diebold, T. Sun, and M. I. Khan, "Photoacoustic monopole radiation in one, two, and three dimensions," *Phys. Rev. Lett.*, vol. 67, pp. 3384–3387, Dec. 1991.

[9] L. Xiang, B. Wang, L. Ji, and H. Jiang, "4-D photoacoustic tomography," *Sci. Rep.*, vol. 3, pp. 01113-1–01113-8, Jan. 2013.

[10] P. N. T. Wells, "Ultrasound imaging," *Phys. Med. Biol.*, vol. 51, pp. R83–R98, Jun. 2006.

[11] A. Fenster and D. B. Downey, "3-D ultrasound imaging: A review," *IEEE Eng. Med. Biol. Mag.*, vol. 15, no. 6, pp. 41–51, Nov./Dec. 1996.

[12] A. P. Jathoul, J. Laufer, O. Ogunlade, B. Treeby, B. Cox, E. Zhang *et al.*, "Deep in vivo photoacoustic imaging of mammalian tissues using a tyrosinase-based genetic reporter," *Nature Photon.*, vol. 9, pp. 239–246, Mar. 2015.

[13] M. Nasiriavanaki, J. Xia, H. Wan, A. Q. Bauer, J. P. Culver, and L. V. Wang, "High-resolution photoacoustic tomography of resting-state functional connectivity in the mouse brain," *Proc. Nat. Academy Sci.*, vol. 111, pp. 21–26, Jan. 2014.

[14] J. Yao, L. Wang, J.-M. Yang, K. I. Maslov, T. T. W. Wong, L. Li *et al.*, "High-speed label-free functional photoacoustic microscopy of mouse brain in action," *Nature Methods*, vol. 12, pp. 407–410, Mar. 2015.

[15] H.-W. Wang, N. Chai, P. Wang, S. Hu, W. Dou, D. Umulis *et al.*, "Label-free bond-selective imaging by listening to vibrationally excited molecules," *Phys. Rev. Lett.*, vol. 106, pp. 238106-1–238106-4, Jun. 2011.

[16] G. Xu, Z.-X. Meng, J. D. Lin, J. Yuan, P. L. Carson, B. Joshi *et al.*, "The functional pitch of an organ: Quantification of tissue texture with photoacoustic spectrum analysis," *Radiol.*, vol. 271, pp. 248–254, Jan. 2014.

[17] X. Wang, Y. Pang, G. Ku, X. Xie, G. Stoica, and L. V. Wang, "Noninvasive laser-induced photoacoustic tomography for structural and functional in vivo imaging of the brain," *Nature Biotechnol.*, vol. 21, pp. 803–806, Jun. 2003.

[18] H. F. Zhang, K. Maslov, G. Stoica, and L. V. Wang, "Functional photoacoustic microscopy for high-resolution and noninvasive in vivo imaging," *Nature Biotech.*, vol. 24, pp. 848–851, Jun. 2006.

[19] R. Nuster, N. Schmitner, G. Wurzinger, S. Gratt, W. Salvenmoser, D. Meyer *et al.*, "Hybrid photoacoustic and ultrasound section imaging with optical ultrasound detection," *J. Biophoton.*, vol. 6, pp. 549–559, May 2013.

[20] K. Jansen, G. V. Soest, and A. F. W. V. d. Steen, "Intravascular photoacoustic imaging: A new tool for vulnerable plaque identification," *Ultrasound Med. Biol.*, vol. 40, pp. 1037–1048, Jun. 2014.

[21] T. F. Fehm, X. L. Deán-Ben, and D. Razansky, "Four dimensional hybrid ultrasound and optoacoustic imaging via passive element optical excitation in a hand-held probe," *Appl. Phys. Lett.*, vol. 105, p. 173505, Sep. 2014.

[22] J. Joseph, V. M. Murukeshan, K. Sathiyamoorthy, and W. L. Sun, "Coherent fiber bundle based integrated photoacoustic, ultrasound and fluorescence imaging (PAUSFI) for endoscopy and diagnostic bio-imaging applications," *Laser Phys.*, vol. 24, pp. 085608-1–085608-7, Jul. 2014.

[23] J. James, V. M. Murukeshan, and L. S. Woh, "Integrated photoacoustic, ultrasound and fluorescence platform for diagnostic medical imaging-proof of concept study with a tissue mimicking phantom," *Biomed. Opt. Exp.*, vol. 5, pp. 2135–2144, Jul. 2014.

[24] S.-L. Chen, Z. Xie, L. J. Guo, and X. Wang, "A fiber-optic system for dual-modality photoacoustic microscopy and confocal fluorescence microscopy using miniature components," *Photoacoustics*, vol. 1, pp. 30–35, May 2013.

[25] Y. Wang, S. Hu, K. Maslov, Y. Zhang, Y. Xia, and L. V. Wang, "In vivo integrated photoacoustic and confocal microscopy of hemoglobin oxygen saturation and oxygen partial pressure," *Opt. Lett.*, vol. 36, pp. 1029–1031, Apr. 2011.

[26] W. Yu, K. Maslov, K. Chulhong, H. Song, and L. V. Wang, "Integrated photoacoustic and fluorescence confocal microscopy," *IEEE Trans. Biomed. Eng.*, vol. 57, no. 10, pp. 2576–2578, Jul. 2010.

[27] C. Zhang, K. Maslov, J. Yao, and L. V. Wang, "In vivo photoacoustic microscopy with 7.6-μm axial resolution using a commercial 125-MHz ultrasonic transducer," *J. Biomed. Opt.*, vol. 17, pp. 116016–116016, Nov. 2012.

[28] S. L. Chen, S. W. Huang, T. Ling, S. Ashkenazi, and L. J. Guo, "Polymer microring resonators for high-sensitivity and wideband photoacoustic imaging," *IEEE Trans. Ultrason., Ferroelect., Freq. Control*, vol. 56, no. 11, pp. 2482–2491, Nov. 2009.

[29] R. E. Davidsen and S. W. Smith, "Two-dimensional arrays for medical ultrasound using multilayer flexible circuit interconnection," *IEEE Trans. Ultrason., Ferroelect., Freq. Control*, vol. 45, no. 2, pp. 338–348, Mar. 1998.

[30] F. S. Foster, K. A. Harasiewicz, and M. D. Sherar, "A history of medical and biological imaging with polyvinylidene fluoride (PVDF) transducers," *IEEE Trans. Ultrason., Ferroelect., Freq. Control*, vol. 47, no. 2, pp. 1363–1371, Jan. 2000.

[31] L. Wang, K. Maslov, J. Yao, B. Rao, and L. V. Wang, "Fast voice-coil scanning optical-resolution photoacoustic microscopy," *Opt. Lett.*, vol. 36, pp. 139–141, Jan. 2011.

[32] K. Maslov, H. F. Zhang, S. Hu, and L. V. Wang, "Optical-resolution photoacoustic microscopy for in vivo imaging of single capillaries," *Opt. Lett.*, vol. 33, pp. 929–931, May 2008.

[33] C. Zhang, K. Maslov, S. Hu, R. Chen, Q. Zhou, K. K. Shung *et al.*, "Reflection-mode submicron-resolution in vivo photoacoustic microscopy," *J. Biomed. Opt.*, vol. 17, pp. 0205011–0205014, Feb. 2012.

[34] Z. Qiu, S. Khondee, X. Duan, H. Li, M. J. Mandella, B. P. Joshi *et al.*, "Vertical cross-sectional imaging of colonic dysplasia in vivo with multispectral dual axes confocal endomicroscopy," *Gastroenterology*, vol. 146, pp. 615–617, Mar. 2014.

[35] B. Wang, J. L. Su, J. Amirian, S. H. Litovsky, R. Smalling, and S. Emelianov, "Detection of lipid in atherosclerotic vessels using ultrasound-guided spectroscopic intravascular photoacoustic imaging," *Opt. Exp.*, vol. 18, pp. 4889–4897, Mar. 2010.

[36] B.-Y. Hsieh, S.-L. Chen, T. Ling, L. J. Guo, and P.-C. Li, "Integrated intravascular ultrasound and photoacoustic imaging scan head," *Opt. Lett.*, vol. 35, pp. 2892–2894, Sep. 2010.

[37] T. Ling, S.-L. Chen, and L. J. Guo, "High-sensitivity and wide-directivity ultrasound detection using high Q polymer microring resonators," *Appl. Phys. Lett.*, vol. 98, p. 204103, May 2011.

[38] P. Morris, A. Hurrell, A. Shaw, E. Zhang, and P. Beard, "A Fabry–Pérot fiber-optic ultrasonic hydrophone for the simultaneous measurement of temperature and acoustic pressure," *J. Acoust. Soc. Amer.*, vol. 125, pp. 3611–3622, Jun. 2009.

[39] A. Maxwell, S.-W. Huang, L. Tao, K. Jin-Sung, S. Ashkenazi, and L. J. Guo, "Polymer microring resonators for high-frequency ultrasound detection and imaging," *IEEE J. Sel. Topics Quantum Electron.*, vol. 14, no. 1, pp. 191–197, Jan./Feb. 2008.

[40] R. Ellwood, E. Zhang, P. Beard, and B. Cox, "Orthogonal Fabry–Pérot sensor array system for minimal-artifact photoacoustic tomography," *Proc. SPIE*, vol. 9323, pp. 932312-1–932312-5, Mar. 2015.

[41] P. K. Kyu, O. Oralkan, and B. T. Khuri-Yakub, "A comparison between conventional and collapse-mode capacitive micromachined ultrasonic transducers in 10-MHz 1-D arrays," *IEEE Trans. Ultrason., Ferroelect., Freq. Control*, vol. 60, no. 6, pp. 1245–1255, Jun. 2013.

[42] J. W. Choe, O. Oralkan, A. Nikoozadeh, M. Gencel, D. N. Stephens, M. O'Donnell, "Volumetric real-time imaging using a CMUT ring array," *IEEE Trans. Ultrason., Ferroelect., Freq. Control*, vol. 59, no. 6, pp. 1201–1211, Jun. 2012.

[43] J. E. Heebner, R. Grover, and T. A. Ibrahim, *Optical Microresonators: Theory, Fabrication, and Applications*. New York, NY, USA: Springer, 2008.

[44] B. E. A. Saleh and T. M. Carl, *Fundamentals of Photonics*. Hoboken, NJ, USA: Wiley, 2007.

[45] C. Zhang, S. Chen, T. Ling, and L. J. Guo, "Review of imprinted polymer microrings as ultrasound detectors: Design, fabrication, and characterization," *IEEE Sensors J.*, vol. 15, no. 6, pp. 3241–3248, Apr. 2015.

[46] L. J. Guo, "Nanoimprint lithography: Methods and material requirements," *Adv. Mater.*, vol. 19, pp. 495–513, Jan. 2007.

[47] M. D. Henry, C. Welch, and A. Scherer, "Techniques of cryogenic reactive ion etching in silicon for fabrication of sensors," *J. Vac. Sci. A*, vol. 27, pp. 1211–1216, Aug. 2009.

[48] S. S. Walavalkar, A. P. Homyk, M. D. Henry, and A. Scherer, "Three-dimensional etching of silicon for the fabrication of low-dimensional and suspended devices," *Nanoscale*, vol. 5, pp. 927–931, Dec. 2013.

[49] H. C. Liu, Y. H. Lin, and W. Hsu, "Sidewall roughness control in advanced silicon etch process," *Microsyst. Technol.*, vol. 10, pp. 29–34, Dec. 2003.

[50] T. Ling, S. L. Chen, and L. J. Guo, "Fabrication and characterization of high Q polymer micro-ring resonator and its application as a sensitive ultrasonic detector," *Opt. Exp.*, vol. 19, pp. 861–869, Jan. 2011.

[51] C.-Y. Chao and L. J. Guo, "Thermal-flow technique for reducing surface roughness and controlling gap size in polymer microring resonators," *Appl. Phys. Lett.*, vol. 84, pp. 2479–2481, Feb. 2004.

[52] C. Zhang, T. Ling, S. L. Chen, and L. J. Guo, "Ultrabroad bandwidth and highly sensitive optical ultrasonic detector for photoacoustic imaging," *ACS Photon.*, vol. 1, pp. 1093–1098, Nov. 2014.

[53] S. L. Chen, T. Ling, and L. J. Guo, "Low-noise small-size microring ultrasonic detectors for high-resolution photoacoustic imaging," *J. Biomed. Opt.*, vol. 16, pp. 056001-1–056001-6, May 2011.

[54] A. S. Erguri, H. Yongli, Z. Xuefeng, O. Oralkan, G. G. Yarahoglu, and B. T. Khuri-Yakub, "Capacitive micromachined ultrasonic transducers: Fabrication technology," *IEEE Trans. Ultrason., Ferroelect., Freq. Control*, vol. 52, no. 12, pp. 2242–2258, Dec. 2005.

[55] O. Oralkan, A. S. Ergun, J. A. Johnson, M. Karaman, U. Demirci, K. Kaviani *et al.*, "Capacitive micromachined ultrasonic transducers: Next-generation arrays for acoustic imaging?," *IEEE Trans. Ultrason., Ferroelect., Freq. Control*, vol. 49, no. 11, pp. 1596–1610, Nov. 2002.

[56] A. Bhuyan, C. J. Woo, L. B. Chul, I. O. Wygant, A. Nikoozadeh, O. Oralkan *et al.*, "Integrated Circuits for volumetric ultrasound imaging with 2-D CMUT arrays," *IEEE Trans. Biomed. Circuits Syst.*, vol. 7, no. 6, pp. 796–804, Jan. 2014.

[57] J. G. Knight and F. L. Degertekin, "Capacitive micromachined ultrasonic transducers for forward looking intravascular imaging arrays," in *Proc. IEEE Ultrason. Symp.*, Munich, Germany, 2002, vol. 2, pp. 1079–1082.

[58] W. J. Westerveld, "Silicon photonic micro-ring resonators to sense strain and ultrasound," Ph.D. dissertation, Dept. Imaging Physics, Delft Univ. Technol., Delft, The Netherlands, 2014.

[59] E. Hallynck and P. Bienstman, "Integrated optical pressure sensors in silicon-on-insulator," *IEEE Photon. J.*, vol. 4, no. 2, pp. 443–450, Apr. 2012.

[60] A. Rosenthal, M. Omar, H. Estrada, S. Kellnberger, D. Razansky, and V. Ntziachristos, "Embedded ultrasound sensor in a silicon-on-insulator photonic platform," *Appl. Phys. Lett.*, vol. 104, p. 021116, Jan. 2014.

[61] F. Monifi, P. Bo, S. K. Ozdemir, M. Lijun, K. Maslov, L. V. Wang, and L. Yang, "Ultrasound sensing using a fiber coupled silica microtoroid resonator encapsulated in a polymer," in *Proc. IEEE Photon. Conf.*, 2013, pp. 215–216.

[62] S. Ashkenazi, Y. Hou, T. Buma, and M. O'Donnell, "Optoacoustic imaging using thin polymer étalon," *Appl. Phys. Lett.*, vol. 86, p. 134103, Mar. 2005.

[63] Y. Hou, S.-W. Huang, R. Witte, M. O'Donnell, and S. Ashkenazi, "Thin polymer etalon arrays for high-resolution photoacoustic imaging," *J. Biomed. Opt.*, vol. 13, pp. 064033-1–064033-8, Nov. /Dec. 2008.

[64] S. W. Huang, Y. Hou, S. Ashkenazi, and M. O'Donnell, "High-resolution ultrasonic imaging using an etalon detector array," *Appl. Phys. Lett.*, vol. 93, p. 113501, Sep. 2008.

[65] N. Huynh, E. Zhang, M. Betcke, S. Arridge, P. Beard, and B. Cox, "A real-time ultrasonic field mapping system using a Fabry–Pérot single pixel camera for 3D photoacoustic imaging," *Proc. SPIE*, vol. 9323, pp. 93231O-1–93231O-7, Mar. 2015.

[66] P. Hajireza, J. Sorge, M. Brett, and R. Zemp, "In vivo optical resolution photoacoustic microscopy using glancing angle-deposited nanostructured Fabry–Perot etalons," *Opt. Lett.*, vol. 40, pp. 1350–1353, Apr. 2015.

[67] P. Hajireza, K. Krause, M. Brett, and R. Zemp, "Glancing angle deposited nanostructured film Fabry–Perot etalons for optical detection of ultrasound," *Opt. Exp.*, vol. 21, pp. 6391–6400, Mar. 2013.

[68] R. J. Colchester, E. Z. Zhang, C. A. Mosse, P. C. Beard, I. Papakonstantinou, and A. E. Desjardins, "Broadband miniature optical ultrasound probe for high resolution vascular tissue imaging," *Biomed. Opt. Exp.*, vol. 6, pp. 1502–1511, Apr. 2015.

[69] E. Z. Y. Zhang and P. C. Beard, "Ultrahigh-sensitivity wideband Fabry–Perot ultrasound sensors as an alternative to piezoelectric PVDF transducers for biomedical photoacoustic detection," *Proc. SPIE*, vol. 5320, pp. 222–229, Jul. 2004.

[70] E. Zhang, J. Laufer, and P. Beard, "Backward-mode multiwavelength photoacoustic scanner using a planar Fabry–Perot polymer film ultrasound sensor for high-resolution three-dimensional imaging of biological tissues," *Appl. Opt.*, vol. 47, pp. 561–577, Feb. 2008.

[71] G. Paltauf, R. Nuster, M. Haltmeier, and P. Burgholzer, "Photoacoustic tomography using a Mach–Zehnder interferometer as an acoustic line detector," *Appl. Opt.*, vol. 46, pp. 3352–3358, Jun. 2007.

[72] R. Nuster, H. Gruen, B. Reitinger, P. Burgholzer, S. Gratt, K. Passler *et al.*, "Downstream Fabry–Perot interferometer for acoustic wave monitoring in photoacoustic tomography," *Opt. Lett.*, vol. 36, pp. 981–983, Mar. 2011.

[73] A. Hochreiner, T. Berer, H. Grün, M. Leitner, and P. Burgholzer, "Photoacoustic imaging using an adaptive interferometer with a photorefractive crystal," *J. Biophoton.*, vol. 5, pp. 508–517, Feb. 2012.

[74] Y. Wang, C. Li, and R. K. Wang, "Noncontact photoacoustic imaging achieved by using a low-coherence interferometer as the acoustic detector," *Opt. Lett.*, vol. 36, pp. 3975–3977, Oct. 2011.

[75] C. Blatter, B. Grajciar, P. Zou, W. Wieser, A.-J. Verhoef, R. Huber *et al.*, "Intrasweep phase-sensitive optical coherence tomography for noncontact optical photoacoustic imaging," *Opt. Lett.*, vol. 37, pp. 4368–4370, Nov. 2012.

[76] G. Gutierrez-Juarez, S. K. Gupta, M. Al-Shaer, L. Polo-Parada, P. S. Dale, C. Papageorgio *et al.*, "Detection of melanoma cells in vitro using an optical detector of photoacoustic waves," *Lasers Surg. Med.*, vol. 42, pp. 274–281, Mar. 2010.

[77] M. Xu and L. V. Wang, "Photoacoustic imaging in biomedicine," *Rev. Sci. Instrum.*, vol. 77, pp. 041101-1–041101-22, Apr. 2006.

[78] S. Park, C. Lee, J. Kim, and C. Kim, "Acoustic resolution photoacoustic microscopy," *Biomed. Eng. Lett.*, vol. 4, pp. 213–222, Sep. 2014.

[79] Z. Xie, S. L. Chen, T. Ling, L. J. Guo, P. L. Carson, and X. Wang, "Pure optical photoacoustic microscopy," *Opt. Exp.*, vol. 19, pp. 9027–9034, May 2011.

[80] J. M. Yang, K. Maslov, H.-C. Yang, Q. Zhou, K. K. Shung, and L. V. Wang, "Photoacoustic endoscopy," *Opt. Lett.*, vol. 34, pp. 1591–1593, May 2009.

[81] A. B. Karpiouk, B. Wang, and S. Y. Emelianov, "Development of a catheter for combined intravascular ultrasound and photoacoustic imaging," *Rev. Sci. Instrum.*, vol. 81, pp. 014901-1–014901-7, Jan. 2010.

[82] K. Jansen, A. F. W. V. D. Steen, H. M. M. V. Beusekom, J. W. Oosterhuis, and G. V. Soest, "Intravascular photoacoustic imaging of human coronary atherosclerosis," *Opt. Lett.*, vol. 36, pp. 597–599, Mar. 2011.
[83] B. Y. Hsieh, S.-L. Chen, T. Ling, L. J. Guo, and P. C. Li, "All-optical scanhead for ultrasound and photoacoustic dual-modality imaging," *Opt. Exp.*, vol. 20, pp. 1588–1596, Jan. 2012.
[84] S. L. Chen, Z. Xie, T. Ling, L. J. Guo, X. Wei, and X. Wang, "Miniaturized all-optical photoacoustic microscopy based on microelectromechanical systems mirror scanning," *Opt. Lett.*, vol. 37, pp. 4263–4265, Oct. 2012.
[85] S. L. Chen, T. Ling, H. W. Baac, and L. J. Guo, "Photoacoustic endoscopy using polymer microring resonators," *Proc. SPIE*, vol 7899, pp. 78992T-1–78992T-6, Feb. 2011.
[86] E. I. Galanzha and V. P. Zharov, "Photoacoustic flow cytometry," *Methods*, vol. 57, pp. 280–296, Jul. 2012.
[87] V. P. Zharov, E. I. Galanzha, E. V. Shashkov, N. G. Khlebtsov, and V. V. Tuchin, "In vivo photoacoustic flow cytometry for monitoring of circulating single cancer cells and contrast agents," *Opt. Lett.*, vol. 31, pp. 3623–3625, Dec. 2006.
[88] L. Wang, K. Maslov, and L. V. Wang, "Single-cell label-free photoacoustic flowoxigraphy in vivo," *Proc. Nat. Acad. Sci.*, vol. 110, pp. 5759–5764, Apr. 2013.
[89] S. L. Chen, T. Ling, S.-W. Huang, H. W. Baac, and L. J. Guo, "Photoacoustic correlation spectroscopy and its application to low-speed flow measurement," *Opt. Lett.*, vol. 35, pp. 1200–1202, Apr. 2010.
[90] S. L. Chen, Y. C. Chang, C. Zhang, J. G. Ok, T. Ling, M. T. Mihnev *et al.*, "Efficient real-time detection of terahertz pulse radiation based on photoacoustic conversion by carbon nanotube nanocomposite," *Nature Photon.*, vol. 8, pp. 537–542, May 2014.
[91] S. L. Chen, C. Zhang, Y.-C. Chang, J. G. Ok, T. Ling, M. T. Mihnev *et al.*, "Efficient real-time detection of terahertz pulse radiation by "Listening to" photoacoustic generation," presented at the Frontiers Optics, Tucson, AZ, USA, 2014, Paper LTh4I.1.
[92] C. Winnewisser, P. U. Jepsen, M. Schall, V. Schyja, and H. Helm, "Electro-optic detection of THz radiation in $LiTaO_3$, $LiNbO_3$ and ZnTe," *Appl. Phys. Lett.*, vol. 70, pp. 3069–3071, Apr. 1997.
[93] H. Shi, J. G. Ok, H. W. Baac, and L. J. Guo, "Low density carbon nanotube forest as an index-matched and near perfect absorption coating," *Appl. Phys. Lett.*, vol. 99, p. 211103, Nov. 2011.
[94] H. W. Baac, J. G. Ok, H. J. Park, T. Ling, S. L. Chen, A. J. Hart *et al.*, "Carbon nanotube composite optoacoustic transmitters for strong and high frequency ultrasound generation," *Appl. Phys. Lett.*, vol. 97, p. 234104, Dec. 2010.
[95] H. W. Baac, J. G. Ok, A. Maxwell, K.-T. Lee, Y.-C. Chen, A. J. Hart *et al.*, "Carbon-nanotube optoacoustic lens for focused ultrasound generation and high-precision targeted therapy," *Sci. Rep.*, vol. 2, pp. 00989-1–00989-8, Dec. 2012.
[96] H. Parsin, S. Wei, and Z. Roger, "Label-free in vivo GRIN-lens optical resolution photoacoustic micro-endoscopy," *Laser Phys. Lett.*, vol. 10, pp. 055603-1–055603-4, Apr. 2013.

Cheng Zhang received B.S. degree in electrical engineering from Shandong University, China in 2010 and is currently a Ph.D. candidate in electrical engineering at the University of Michigan, Ann Arbor, MI, USA. His research interest includes polymer based photonic devices, plasmonics and metamaterials. He is a student member of IEEE, OSA and SPIE.

Sung-Liang Chen received the B.S. degree in electrical engineering and the M.S. degree in electrooptical engineering from National Taiwan University, Taipei, Taiwan, in 2003 and 2005, respectively, and the Ph.D. degree in electrical engineering from the University of Michigan, Ann Arbor, MI, USA, in 2011. He had the postdoctoral training at the University of Michigan Medical School. He is currently an Assistant Professor at the University of Michigan-Shanghai Jiao Tong University Joint Institute, Shanghai, China. His research interests include optical resonators for sensing applications, optical imaging systems, and PAI.

Tao Ling received the B.S. degree in physics from Nankai University, Tianjin, China, the M.S. degree in optics from Fudan University, Shanghai, China, and the Ph.D. degree in electrical engineering from the University of Michigan, Ann Arbor, MI, USA. He is currently an Electro-Optical Engineer in TE Connectivity working on single mode and multimode transceiver development.

L. Jay Guo started his academic career at the University of Michigan as an assistant professor in 1999, and is currently a professor in the Department of Electrical Engineering and Computer Science. He directs an interdisciplinary lab at the intersection of electrical engineering, photonics, polymer materials and mechanical engineering. His group's researches include polymer-based photonic devices and sensor applications, organic and hybrid photovoltaics, plasmonic nano-photonics, scalable nano-manufacturing technologies such as roll to roll nano-imprinting.